Microsystem Technologies
https://doi.org/10.1007/s00542-019-04743-2

TECHNICAL PAPER

Optimization of a synthetic jet based piezoelectric air pump and its application in electronic cooling

Cheng Liu[1] · Yuchuan Zhu[1] · Changwen Wu[1]

Received: 3 September 2019 / Accepted: 27 December 2019

Abstract
In this paper, the optimization is carried out for a synthetic jet based piezoelectric air pump. The structural parameters which affect the output flowrate are determined and orthogonal test method is used to find out the optimal values of these parameters. Driven by a 150 Vpp, 3.15 kHz sinusoidal voltage signal, the optimized pump reaches its maximum output flowrate of 2.79 L/min, which is 32.9% higher than that before optimization. Using the synthetic jet based piezoelectric air pump as gas source, an open-loop detection and closed-loop control system is built for electronic cooling. The open-loop experiments show that the heater's surface temperature can be maintained at around 97.9 °C when the cooling distance is 60 mm, which is 32.5% lower than the initial value. The closed-loop control system can limit the temperature within the set interval. Both the open and closed-loop system show that the synthetic jet based piezoelectric air pump has application prospects in the field of electronic cooling.

1 Introduction

Piezoelectric material is a kind of typical smart material. Pumps using piezoelectric material as driving component are widely used in drug delivery (Revathi and Padmanabhan 2016; Sateesh et al. 2018) and biochemical analysis (Ma et al. 2016) due to their small size and fast response, but the small output flowrate limit their application in other areas. Since professor Ari Glezer found the synthetic jet in 1998 (Smith and Glezer 1998), this special fluid phenomenon with high strength and continuous output flow has received extensive attention and has been applied in many fields such as active flow control (Okada et al. 2012; Fisher et al. 2017) and mixing enhancement (Wang et al. 2018). The synthetic jet based piezoelectric pumps combine the advantages of both the piezoelectric material and the synthetic jet, which overcome the shortage of the conventional piezoelectric pumps. In recent years, some scholars have explored the application of synthetic jet devices in the field of heat transfer (Jalilvand et al. 2015; Ghaffari et al. 2016; Deng et al. 2017), showing a promising development prospect.

Any product that wants to be applied in a real scene requires a lot of optimization to get it working at its best. There are two main optimization methods, one is to adjust the size of the existing structure, the other is to introduce a new structure or principle. In the field of piezoelectric pump, many scholars have studied the possibility of improving the output performance by adding more driving components, pump chambers and changing the flow channel design (He et al. 2016; Dong et al. 2017). However, the increase of new components and structures may also lead to negative effects such as more power consumption, and trade-offs are needed. As for the adjustment of the structural size, especially in the case of multiple influencing factors, there are also problems of excessive experimental combinations and costs. Therefore, it is necessary to reduce the number of experiments under the premise of ensuring certain accuracy through scientific methods. The orthogonal test method is relatively common and practical method. Many scholars use this method to complete the performance optimization of the research object (Yuan et al. 2015; Alrashdan et al. 2015; Xu et al. 2017).

✉ Yuchuan Zhu
meeyczhu@nuaa.edu.cn

Cheng Liu
liucheng_nuaa@163.com

Changwen Wu
15059273865@163.com

[1] National Key Laboratory of Science and Technology on Helicopter Transmission, Nanjing University of Aeronautics and Astronautics, Nanjing 210016, China

Published online: 04 January 2020

In order to optimize the structure of the synthetic jet based piezoelectric air pump, improve its output flowrate and then meet the application needs of electronic cooling, the main contents of this paper are:

1. Find the key structural parameters which have influence on the pump's output flowrate, and initially determine the approximate range of the optimal parameters.
2. Optimize the synthetic jet based piezoelectric air pump by orthogonal test method, find a set of parameters corresponding to the maximum output flowrate and obtain the degree of influence of each structural parameter on the output flowrate.
3. Set up a specific application scene for the optimized piezoelectric pump to explore its prospects in the field of electronic cooling. The main goals are to find out its optimal cooling status, ultimate cooling ability and the ability to prevent electronic devices from overheating and large temperature fluctuations.

2 Optimization of the piezoelectric pump

2.1 Piezoelectric air pump to be optimized

In the previous work (Liu and Zhu 2019), a synthetic jet based piezoelectric air pump was designed and manufactured.

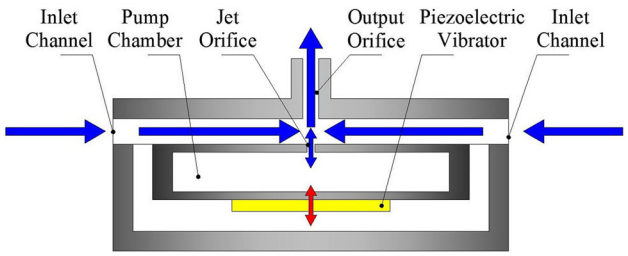

(a) Principle diagram of the piezoelectric pump

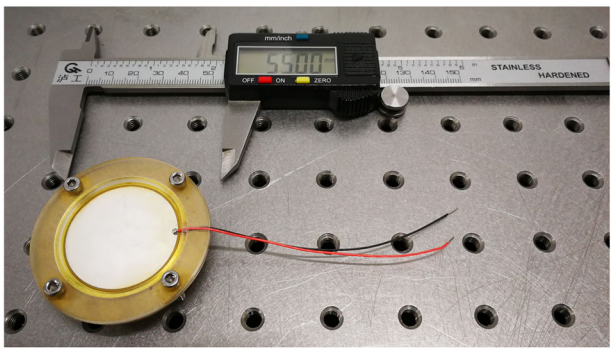

(b) Prototype of the piezoelectric pump

Fig. 1 Principle diagram and prototype of the piezoelectric pump

The principle diagram and the prototype are shown in Fig. 1a, b. The piezoelectric vibrator deforms up and down under a sinusoidal voltage signal, so that the air is sucked into/gets out of the pump chamber. During this periodic process, air around the jet orifice is subjected to intense shear force and then generates vortex pairs. These vortex pairs that move downstream and won't be sucked back to the pump chamber finally create the synthetic jet phenomenon.

The diameter of the piezoelectric vibrator used in this pump is 41 mm. The total diameter of the pump is 55 mm and the thickness without nozzle is 5 mm. The output flowrate can reach up to 2.1 L/min driven by a 150 Vpp, 2.85 kHz sinusoidal voltage signal. This pump is only a prototype for principle proof, but its output flowrate and frequency response are still considerable. Therefore, the optimization of this pump is carried out in order to achieve a higher output flowrate.

2.2 Analysis of the structural parameters affecting the output flowrate

In order to optimize an existing synthetic jet based piezoelectric air pump, it's necessary to find out the key structural parameters that affect its output flowrate and determine the range in which the optimal values may fall.

There are few theoretical analysis on the output flowrate of the synthetic jet based piezoelectric pumps, but there are many on synthetic jets (Tang and Zhong 2006; Persoons et al. 2018). Combined these existing analysis with the actual situation of the pump in this paper, the theoretical expression of the pump's output flowrate can be given.

The theoretical expression can be divided into two parts: part I is the input electrical signal to the output displacement of the vibrator, and part II is the input displacement of the vibrator to the output flowrate of the pump, as shown in Fig. 2.

For part I, the theoretical expression from the input voltage U to the vibrator's central displacement $w(0)$ and then to the vibrator's displacement distribution $w(r)$ has been given in the previous work (Liu and Zhu 2019), as shown in Eq. 1.

$$w(0) = K \times U$$
$$w(r) = \left[1 - \left(\frac{r}{r_v}\right)^2\right] \times w(0) \tag{1}$$

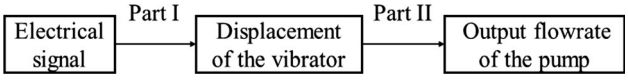

Fig. 2 Theoretical expression of the pump's flowrate

where K is the structural coefficient. r is the distance from any point to the center. When considering the vibration as a dynamic process, w(r) in Eq. 1 can be expressed as Eq. 2.

$$w(r,t) = \left[1 - \left(\frac{r}{r_v}\right)^2\right] \times w(0) \times \sin 2\pi ft \tag{2}$$

where f is the vibration frequency.

For part II, The vibration velocity $u(r, t)$ can be given as Eq. 3.

$$\begin{aligned} u(r,t) &= w(r,t)' \\ &= 2\pi f \times \left[1 - \left(\frac{r}{r_v}\right)^2\right] \times w(0) \times \cos 2\pi ft \end{aligned} \tag{3}$$

The instantaneous flowrate and velocity through the jet orifice are given as Eq. 4.

$$\begin{aligned} \dot{Q}_j(t) &= \rho u_j(t) A = \rho \int_0^{r_v} u(r,t) \times 2\pi r \mathrm{d}r \\ &= \frac{\pi^2}{4} \rho f d_v^2 \times w(0) \times \cos 2\pi ft \\ u_j(t) &= \frac{\dot{Q}_j(t)}{\rho A} = \pi f w(0) \times \left(\frac{d_v}{d_j}\right)^2 \times \cos 2\pi ft \end{aligned} \tag{4}$$

where ρ is the density of the fluid, A is the cross sectional area of the jet orifice. d_v and d_j are the diameter of the vibrator and the jet orifice, respectively. The average velocity and flowrate through the jet orifice in one cycle T are shown as Eq. 5.

$$\begin{aligned} \bar{u}_j &= \frac{1}{T} \int_{T/4}^{-T/4} u_j(t) \mathrm{d}t = \frac{1}{T} \times w(0) \times \left(\frac{d_v}{d_j}\right)^2 \\ \bar{Q}_j &= \frac{1}{T} \int_{T/4}^{-T/4} \dot{Q}_j(t) \mathrm{d}t = \frac{\pi}{4} \rho f \times w(0) \times d_v^2 \end{aligned} \tag{5}$$

It can be seen from the above formulas that the output flowrate of the pump is related to the diameter of the vibrator and the jet orifice. When the vibrator is selected, the diameter of the vibrator and the pump chamber are determined. So the diameter of the jet orifice is the key parameter that affects the output flowrate.

The influence of other parameters on the output flowrate were studied in previous paper (Liu and Zhu 2019). The original dimensions of the prototype for principle proof are: height of the inlet channel h_i = 0.8 mm, height of the pump chamber h_p = 0.3 mm, diameter of the jet orifice d_j = 1.0 mm and diameter of the outlet orifice d_o = 1.5 mm. The optimization work of each parameter were carried out using simulation software, and a set of parameter combinations that maximized the output flowrate under simulation environment was obtained: h_i = 0.6 mm, h_p = 0.5 mm, d_j = 1.2 mm and d_o = 1.9 mm. Based on these work, the structural parameters need to be optimized in this paper can be determined, as well as the range in which the optimal values of the structural parameters fall, as shown in Fig. 3 and Table 1.

2.3 Optimization using orthogonal test method

The key parameters affecting the output flowrate have been listed in Table 1, Sect. 2.2. For this kind of optimization work with multiple influencing factors, orthogonal test method is an effective method. The orthogonal test method uses a set of standardized tables, i.e., orthogonal tables, to design experimental schemes and analyze experimental results. Its core is to use a few representative combinations to reflect all situations and find out the optimal result.

There are several basic information to be determined first. The optimization problem is a single indicator problem, the output flowrate is the only indicator. There are four key structural parameters affecting the output flowrate, that is, the "factors" in orthogonal test: inlet channel height h_i, pump chamber height h_p, jet orifice diameter d_j and outlet orifice diameter d_o. Each factor has three values as the "levels" in orthogonal test. The factors and levels are shown in Table 2.

The second step is to select the appropriate orthogonal table. For the 4-factor, 3-level problem, the $L_9(3^4)$ orthogonal table meets the requirement. There are still some other problems: the theoretical analysis is based on the situation under the first order resonant frequency, and the frequency corresponding to the maximum output flowrate obtained by different test combinations are not the same. Therefore, the output flowrate under the frequency of 1000 Hz is selected as the results in orthogonal table. A hypothesis is made: the pump which has a higher output flowrate near the first order resonant frequency will also has a higher maximum output flowrate. The tests also record the maximum output flowrate and the corresponding frequency to verify this hypothesis.

The test combinations and the results are shown in Table 3. K_i corresponds to the sum of the test results of each factor and the level is i. k_i is the average of K_i, that is, $k_i = K_i$/level number. R is the extreme difference, i.e., the difference between the maximum and minimum value of k_i. From Table 3, two conclusions can be drawn: (1) The primary-second relationship of the factors. The degree of

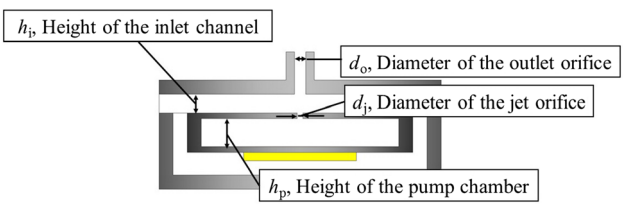

Fig. 3 Diagram of the parameters to be optimized

Table 1 Structural parameters to be optimized

Parameter	Symbol	Value range (mm)
Height of the inlet channel	h_i	0.6–0.8
Height of the pump chamber	h_p	0.3–0.7
Diameter of the jet orifice	d_j	1.0–1.4
Diameter of the outlet orifice	d_o	1.5–1.9

Table 2 Factors and levels of the test

Level	h_i (mm)	h_p (mm)	d_j (mm)	d_o (mm)
1	0.6	0.3	1.0	1.5
2	0.7	0.5	1.2	1.7
3	0.8	0.7	1.4	1.9

influence of each factor on the output flowrate is judged according to value R. It can be seen that $h_p > d_j > h_i > d_o$. (2) The optimal level combination. According to the value of k_i, a set of optimal combination can be obtained: h_i = 0.8 mm, h_p = 0.3 mm, d_j = 1.2 mm and d_o = 1.9 mm. The maximum output flowrate of this combination is found to be 2.38 L/min through the verification experiment, so the optimal combination is still the fourth group in the orthogonal test: h_i = 0.7 mm, h_p = 0.3 mm, d_j = 1.2 mm and d_o = 1.9 mm.

Table 4 Comparison of the output flowrate under 1000 Hz and the maximum output flowrate

Group number	Output flowrate at 1 kHz (L/min)	Maximum output flowrate (L/min)	Corresponding frequency (kHz)
1	0.64	2.48	3.10
2	0.71	1.92	3.05
3	0.56	1.84	3.05
4	1.15	2.79	3.15
5	0.72	2.01	3.05
6	0.50	1.97	1.55
7	0.94	2.58	3.15
8	0.79	2.30	3.05
9	0.76	1.83	1.60

In order to verify the assumption before the tests, the output flowrate at 1 kHz, the maximum output flowrate and corresponding frequency are listed in Table 4. It can be seen that there is a positive correlation between the flowrate near the first order resonant frequency (about 1 kHz) and the maximum flowrate, excluding the test error and some special conditions. Therefore, the assumption before test and the test results are reasonable.

It also can be seen from Table 4 that the maximum output flowrate of the pump mostly appears in the range of 3.05–3.15 kHz. The maximum output flowrate of the prototype before optimization appears at 2.85 kHz, all of them are far higher than the vibrator's first order resonant frequency, but are closed to its second order resonant frequency (about 2.9 kHz).

Table 3 Orthogonal table and results

Group number	Factors				Results
	h_i (mm)	h_p (mm)	d_j (mm)	d_o (mm)	Q (L/min)
1	0.6	0.3	1.0	1.5	0.64
2	0.6	0.5	1.2	1.7	0.71
3	0.6	0.7	1.4	1.9	0.56
4	0.7	0.3	1.2	1.9	1.15
5	0.7	0.5	1.4	1.5	0.72
6	0.7	0.7	1.0	1.7	0.50
7	0.8	0.3	1.4	1.7	0.94
8	0.8	0.5	1.0	1.9	0.79
9	0.8	0.7	1.2	1.5	0.76
K_1	1.91	2.73	1.93	2.12	
K_2	2.37	2.22	2.62	2.15	
K_3	2.49	1.82	2.22	2.50	
k_1	0.637	0.910	0.643	0.707	
k_2	0.790	0.740	0.873	0.717	
k_3	0.830	0.607	0.740	0.833	
R	0.193	0.303	0.230	0.126	

2.4 Results

Through the orthogonal test method, the structural size of the piezoelectric air pump is optimized. The maximum output flowrate of the optimized pump is 2.79 L/min, driven by a 150 Vpp, 3.15 kHz sinusoidal voltage signal, which is 32.9% higher than that before optimization. The comparison of the output flowrate curves of the piezoelectric air pumps before and after the optimization in the frequency range of 0–5 kHz is shown in Fig. 4.

In the existing researches on synthetic jet based piezoelectric pump, some scholars (e.g. Wang 2017) proposed that the optimal working frequency should be lower than the vibrator's first order resonant frequency. But the experiments in this paper found that the optimal working frequency is concentrated in the range of 2.85–3.15 kHz, which is much higher than the vibrator's first order resonant frequency (about 1.1 kHz), and is closed to the second order resonant frequency (about 2.9 kHz). The conclusions can be drawn: the rational use of the resonant frequency can increase the output flowrate, but the working frequency should not be limited under the first order resonant frequency, higher order resonant frequency may lead to higher output flowrate.

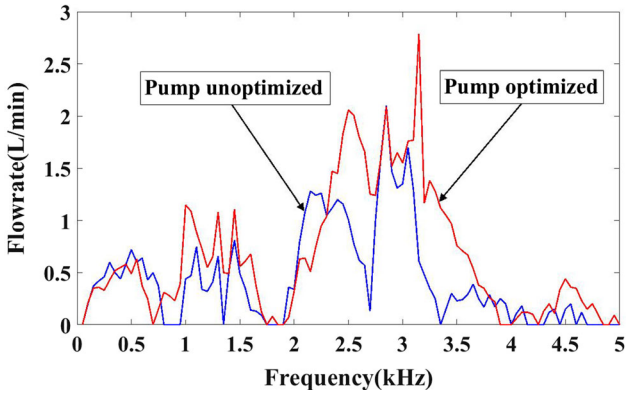

Fig. 4 Flowrate curves of the unoptimized and optimized pumps

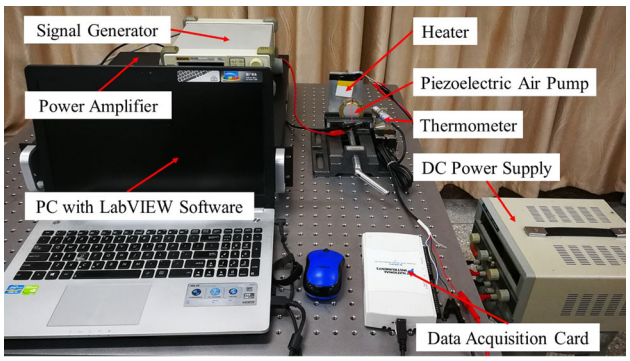

(a) Test bench of the open-loop system

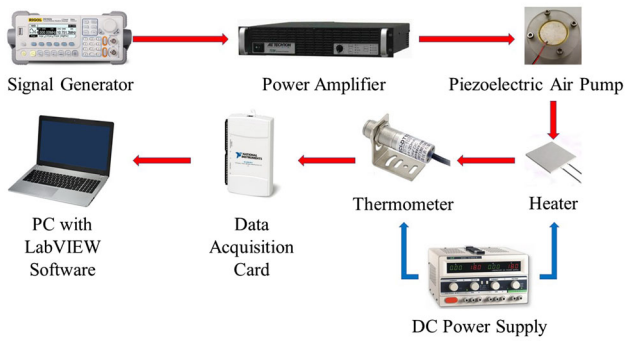

(b) Principle of the open-loop system

Fig. 5 Open-loop thermal detection system

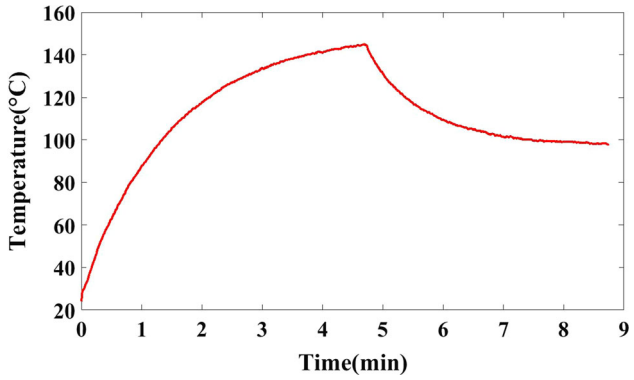

Fig. 6 Temperature curve

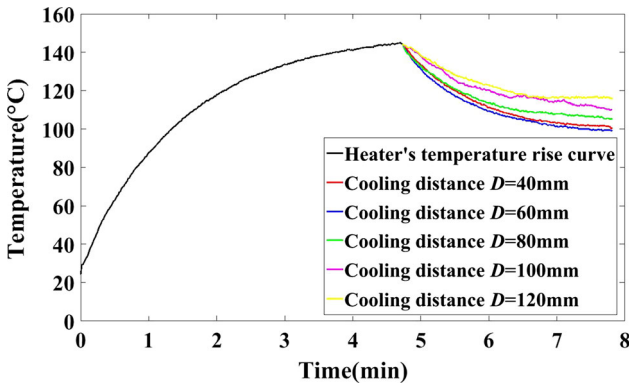

Fig. 7 Temperature curve under different cooling distance

Table 5 Stable temperatures under different cooling distance

Number	Cooling distance (mm)	Stable temperature (°C)
1	40	100.7
2	60	97.9
3	80	105.2
4	100	109.9
5	120	115.8

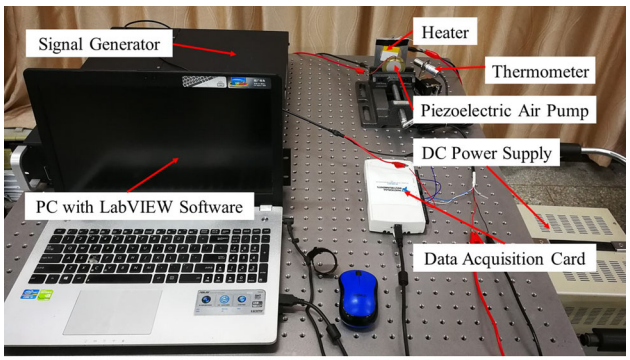

(a) Test bench of the closed-loop system

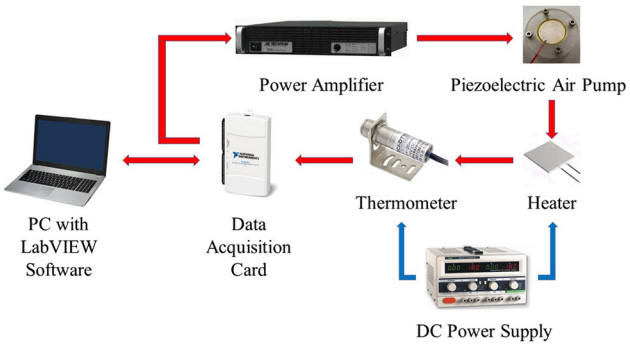

(b) Principle of the closed-loop system

Fig. 8 Closed-loop thermal control system

3 Application of the piezoelectric air pump in electronic cooling

Thermal issues have become significant design factors in electronic devices. Overheating can cause failure of the electronic components and deformation of the mechanical parts. Temperature fluctuations will also lead to significant changes in electronic devices' performance (Memik 2015). Therefore, in this section of cooling application, focus lies on the optimal cooling condition of the synthetic jet based piezoelectric air pump and its ability to prevent overheating and large temperature fluctuations.

Through the work in Sect. 2, the synthetic jet based piezoelectric air pump with optimized structural parameters and the optimal working condition are obtained. In this section, an open-loop detection and closed-loop control system is built for the application in electronic cooling and the optimized pump is used as the gas source.

3.1 Open-loop thermal detection

The test bench and the principle of the open-loop detection system is shown in Fig. 5. The sinusoidal signal that drives the pump is generated by the signal generator (RIGOL DG1022) and amplified by the power amplifier (AE Techron 7224). A heater (XH-RP4040) is used to simulate the heating status of the electronic component. An infrared thermometer (LSCI DT300, range from 0 to 300 °C) is used to measure the surface temperature of the heater. The thermal signal is transferred to PC via data acquisition card

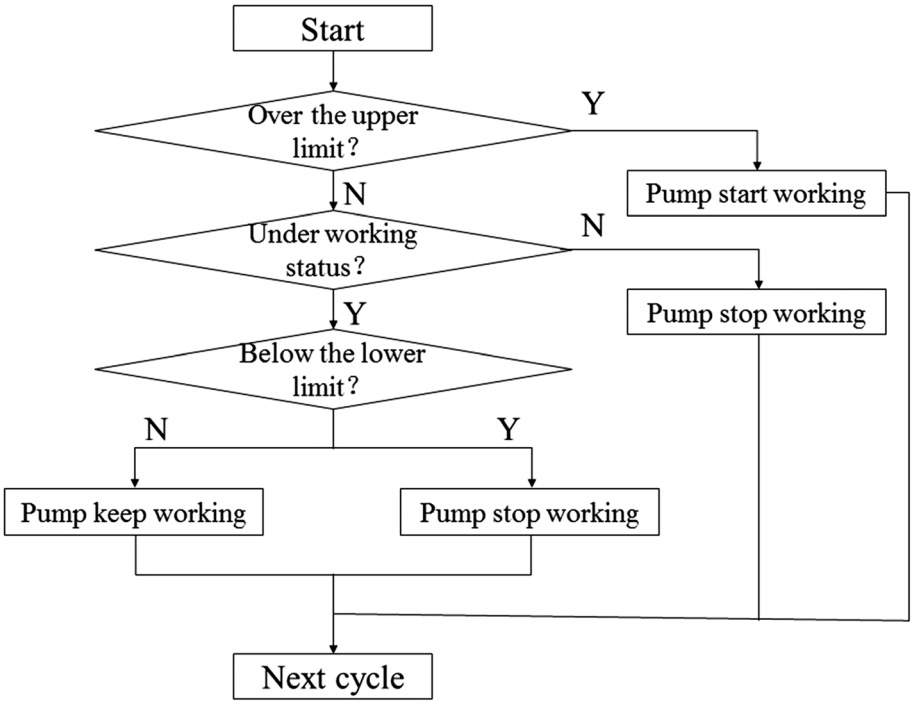

Fig. 9 Flow chart of the control loop

Fig. 10 control loop in LabVIEW software

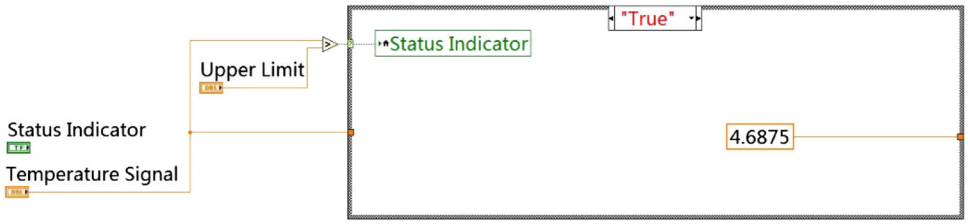

(a) Case 1 of the control loop body

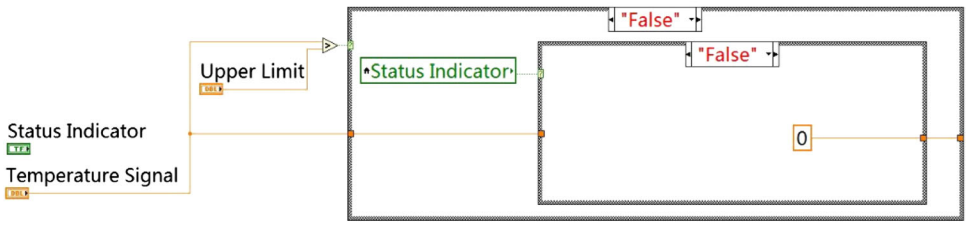

(b) Case 2 of the control loop body

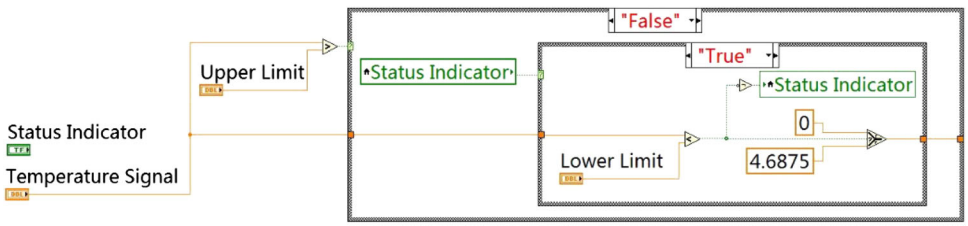

(c) Case 3 of the control loop body

(NI USB 6211) and displayed on the front panel of the LabVIEW software. Both the heater and the thermometer are powered by a DC power supply (QJE QJ3003S).

The typical temperature change curve is shown in Fig. 6. The rated power of the heater used in this test is 16 W. The output power decreases due to the increase of internal resistance after the temperature rises, reflecting on the temperature curve is that the curve's slope becomes smaller. After working 4.7 min, the surface temperature of the heater can be maintained at around 145 °C. When the pump start working, the surface temperature drops and finally maintains at a stable temperature. The difference between this temperature and the maximum temperature (145 °C) can be used to measure the cooling effect of the pump.

The cooling distance, i.e., the distance between the pump's outlet orifice and the heater's surface, is an important parameter which affect the cooling result. By adjusting the cooling distance, a series of temperature curves can be obtained, as shown in Fig. 7.

The cooling distance is selected as 40 mm, 60 mm, 80 mm, 100 mm, 120 mm. The pump doesn't work during the first 4.7 min and starts working when the heater's temperature naturally rises to 145 °C. The operating voltage and frequency are set to 150 Vpp and 3.15 kHz, respectively, which is the optimal working point. It can be seen that as the cooling distance decreases, the final stable temperature also decreases, but the opposite trend occurs when the distance is too close, that is, there has an optimal cooling distance.

The corresponding stable temperatures under different cooling distances are shown in Table 5. When the cooling distance is 60 mm, the system can control the heater's temperature within 100 °C, reaching to 97.9 °C, which is 32.5% lower than the initial value (145 °C). 60 mm is the optimal cooling distance for this system.

3.2 Closed-loop thermal control

Through the open-loop test in Sect. 3.1, the cooling performance of the piezoelectric pump under different cooling distance is obtained. Based on this, a closed-loop control system can be developed to control the heater's surface temperature. The test bench and the principle of the closed-loop control system is shown in Fig. 8.

The instruments are basically the same as the open-loop system. The driving signal is amplified by the power amplifier, the heater's temperature is detected by infrared

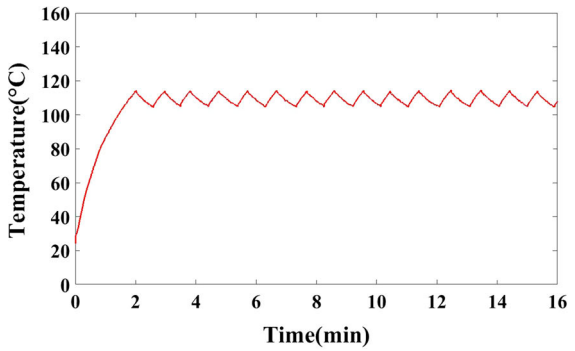

(a) Set range from 105 to 114°C

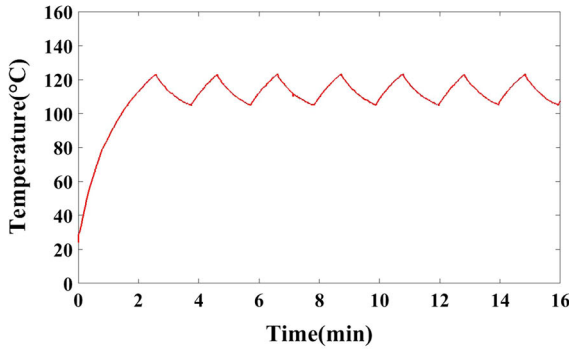

(b) Set range from 105 to 123°C

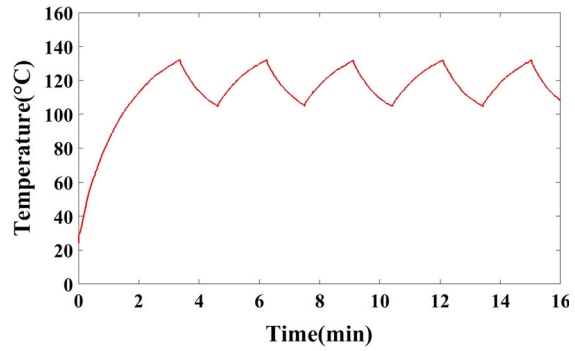

(c) Set range from 105 to 132°C

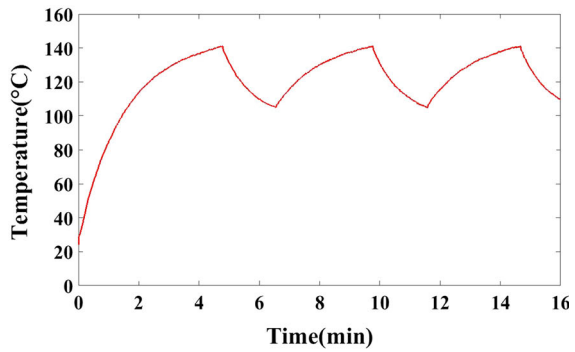

(d) Set range from 105 to 141°C

Fig. 11 Test results of the closed-loop system

thermometer and transfer to PC via data acquisition card. The signal generator used in open-loop system is replaced by the analog output port of the data acquisition card.

In closed-loop control system, it's necessary to judge the detected temperature signal and then generate the corresponding output signal to drive the pump. The most critical part of the whole process is a loop body that detects and processes the temperature signal. The logic flow chart is shown in Fig. 9.

First, it judges whether the temperature exceeds the upper limit. If so, the pump start working directly; If not, it's necessary to further judge whether the pump is working currently. If not, it indicates that the heater's temperature is natural rising so the pump continues the stopped state; If so, it indicates that the heater's temperature is dropping and further judgement whether the temperature is smaller than lower limit is needed. If so, the pump stops working; If not, the pump continues to work. So far is a complete cycle of the control loop. Repeat this cycle, The system will generate the signals according to the thermal signals to control the pump's working state and realize the closed-loop control.

In the LabVIEW software, this loop body is realized by nested case structures, as shown in Fig. 10.

The status indicator is a Boolean control, which not only displays the pump's working status, but also works as an input control of the inner case structure. The temperature signal is first compared with the upper limit. If it's true, as shown in Fig. 10a, the status indicator is also true, the analog output port of the data acquisition card generates a 9.375 Vpp, 3.15 kHz sinusoidal signal. This signal is amplified by the power amplifier for 16 times and becomes the driving signal of the pump. If the comparison result is false, further judge the pump's working status, that is, true of false of the status indicator. If it's false, output 0 directly so the pump stops, as shown in Fig. 10b. If it's true, further compare the temperature signal with the lower limit. If it's true, the status indicator is false and the output signal is 0, the pump stops. If it's false, the status indicator is true and the pump keeps working, as shown in Fig. 10c. The logical judgement process shown in Fig. 9 is realized through this nested case structure.

The thermometer used in this paper has a range of 0–300 °C, corresponding to a 0–5 V voltage output. According to the result of the open-loop detection test, the lower limit voltage in closed-loop control system is set to 1.75 V and the upper limit voltage is set to 1.9 V, 2.05 V, 2.2 V and 2.35 V, that is, the lower limit is set to 105 °C and the upper limit is set to 114 °C, 123 °C, 132 °C and 141 °C, respectively. The test results are shown in Fig. 11.

It can be seen that the closed-loop control system can control the heater's surface temperature effectively. The temperature is kept within the preset upper and lower limit.

Table 6 Pump's work/stop time during each cooling period

No.	Cooling period (s)	Work time (s)	Stop time (s)	Work time ratio (%)
(a)	54.0	32.5	21.5	60.2
(b)	121.0	68.5	52.5	56.6
(c)	172.5	75.0	97.5	43.5
(d)	299.0	106.0	193.0	35.5

Table 7 Control accuracy of the closed-loop system

No.	Set interval (V)	Actual interval (V)	Excess (V)	Temperature excess (°C)
(a)	1.95	1.90981	+ 0.00981	+ 0.5886
	1.75	1.73887	− 0.01113	− 0.6678
(b)	2.05	2.05887	+ 0.00887	+ 0.5322
	1.75	1.74249	− 0.00751	− 0.4506
(c)	2.20	2.20480	+ 0.00480	+ 0.2880
	1.75	1.73756	− 0.01244	− 0.7464
(d)	2.35	2.35452	+ 0.00452	+ 0.2712
	1.75	1.74578	− 0.00422	− 0.2532

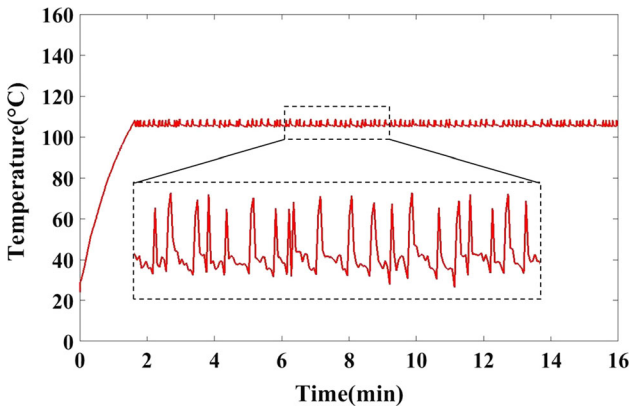

Fig. 12 Temperature curve when the set range is 105 to 108 °C

Defining the time during which the temperature drops from the upper limit to the lower limit and then rises back as a cooling period, the pump's work and stop time during each period can be further obtained, as shown in Table 6.

It can be seen that the pump needs to change the working status more frequently in order to control the temperature in a smaller interval, the cooling period is shorter, but the working time is longer during each cooling period. In other scholar's research (Deng et al. 2017), a closed-loop thermal control using a synthetic jet device with different structure from this paper also has similar conclusions.

In addition, Table 7 shows the control accuracy of the closed-loop system. There are excesses (about 0.5 °C) at both the upper and lower limit. The main reason for these excesses is the response time of the thermometer (about 300 ms).

The excess doesn't change much when the temperature interval changes, so when the set interval is too small, the periodicity of the temperature curve becomes worse, but the temperature can still be controlled within a certain interval, as shown in Fig. 12. The set interval is 1.75–1.80 V.

Through the above thermal open-loop detection and closed-loop control tests, it can be concluded that the cooling system based on piezoelectric air pump can be applied in electronic cooling. The system built in this paper can work normally, collect the thermal signal, generate the corresponding control signal and finally control the heater's surface temperature within the set interval.

4 Conclusions

In this paper, the structural parameters of a synthetic jet based piezoelectric air pump is optimized and the research in electronic cooling field based on this pump is carried out. The main conclusions are as follows:

1. The structural parameters of the synthetic jet based piezoelectric air pump is optimized by orthogonal test method. The degree of influence of each parameter on output flowrate is obtained and optimal parameter combinations are determined. The optimized pump achieves a maximum output flowrate of 2.79 L/min under the excitation of a 150 Vpp, 3.15 kHz sinusoidal voltage signal, which is 32.9% higher than that before optimization.
2. The rational use of the vibrator's resonant frequency will lead to the increase in pump's flowrate. The pump's optimal working frequency achieved at the

range of 2.85–3.15 kHz, which are all closed to the vibrator's second order resonant frequency.

3. An open-loop detection system is built to study the cooling effect of the pump. The test results show that the optimal cooling distance is 60 mm and the stable temperature is 97.9 °C, showing a certain cooling effect.
4. A closd-loop control system is built to verify the feasibility of thermal control based on the pump. The test results show that this system can control the temperature within the set interval, the excess at both the upper and lower limit is about 0.5 °C. The smaller the interval is, the more frequently the pump's working state changes, the shorter the cooling period is and the longer the pump works during each period.

Acknowledgments The authors would like to acknowledge the financial support from the National Science Foundation of China (Grant No. 51575258; 51975275) and the Foundation of Graduate Innovation Center in NUAA (Grant No. kfjj20180503).

References

Alrashdan M, Hamzah A, Majlis B (2015) Design and optimization of cantilever based piezoelectric micro power generator for cardiac pacemaker. Microsyst Technol 21:1607–1617

Deng X, Luo ZB, Xia ZX et al (2017) Active-passive combined and closed-loop control for the thermal management of high-power LED based on a dual synthetic jet actuator. Energy Convers Manag 132:207–212

Dong JS, Chen WH, Zeng P et al (2017) Design and experimental research on piezoelectric pump with triple vibrators. Microsyst Technol 23:3019–3026

Fisher R, Nishino T, Savill M (2017) Numerical analysis of a bidirectional synthetic jet for active flow control. AIAA J 55(3):1064–1069

Ghaffari O, Solovitz SA, Ikhlaq M et al (2016) An investigation into flow and heat transfer of an ultrasonic micro-blower device for electronics cooling applications. Appl Therm Eng 106:881–889

He XH, Xu L, Zhang XT et al (2016) A bidirectional valveless piezoelectric micropump with three chambers applying synthetic jet. J Mech Sci Technol 30(9):4015–4022

Jalilvand A, Mochizuki M, Saito Y et al (2015) Cooling performance evaluation of synthetic jet based thermal solution module. J Therm Sci Eng Appl 7:031010-1–031010-9

Liu C, Zhu YC (2019) Simulation and experimental study of direct spray type piezoelectric air pumps based on synthetic jet. Microsyst Technol 25:4445–4454

Ma HK, Chen RH, Yu NS et al (2016) A miniature circular pump with a piezoelectric bimorph and a disposable chamber for biomedical applications. Sens Actuators A 251:108–118

Memik S (2015) Heat management in integrated circuits: on-chip and system-level monitoring and cooling. Institution of Engineering and Technology, London, pp 1–9

Okada K, Nonomura T, Fujii K et al (2012) Computational analysis of vortex structures induced by a synthetic jet to control separated flows. Int J Flow Control 4:47–66

Persoons T, Cressall R, Alimohammadi S (2018) Validating a reduced-order model for synthetic jet actuators using CFD and experimental data. Actuators 7:1–17

Revathi S, Padmanabhan R (2016) Study of the effect on flow rate for planar type polymer-based diaphragm piezoelectric actuated valveless micropump for insulin delivery. Adv Mater Process Technol 2(1):31–43

Sateesh J, Girija K, Akshay R et al (2018) Design and flow analysis of MEMS based piezo-electric micro pump. Microsyst Technol 24:1609–1614

Smith BL, Glezer A (1998) The formation and evolution of synthetic jets. Phys Fluids 10(9):2281–2297

Tang H, Zhong S (2006) Incompressible flow model of synthetic jet actuators. AIAA J 44(4):908–912

Wang X (2017) Simulation analysis and experimental research of resonant air piezoelectric pump based on synthetic jet. Jilin University, Changchun, China

Wang L, Feng LH, Wang JJ et al (2018) Characteristics and mechanism of mixing enhancement for noncircular synthetic jets at low Reynolds number. Exp Therm Fluid Sci 98:731–743

Xu XM, Li XC, Zhou J et al (2017) Numerical and experimental analysis of cold gas microthruster geometric parameters by univariate and orthogonal method. Microsyst Technol 23:5003–5016

Yuan SQ, Yang S, He XH et al (2015) Design and experimental study of a novel three-way diffuser/nozzle elements employed in valveless piezoelectric micropumps. Br Soc Mech Sci Eng 37:221–230